ACS OMEGA

Open Access

http://pubs.acs.org/journal/acsodf

Article

Bioactive Wound Healing 3D Structure Based on Chitosan Hydrogel Loaded with Naringin/Cyclodextrin Inclusion Nanocomplex

Donghui Bian, Younes Pilehvar, Sanaz Kousha, and Jianhai Bi*

Cite This: *ACS Omega* 2024, 9, 10566−10576

Read Online

ACCESS | Metrics & More | Article Recommendations

ABSTRACT: The current assay aimed to fabricate and analyze a potent wound healing structure based on a naringin (Nar)/β-cyclodextrin (β-CD)-loaded chitosan hydrogel. Using the simulation studies, we assessed the interactions among the Nar, β-CD, and the formation of the inclusion complex. Then, the formation of the hydrogel nanocomplex was simulated and evaluated using the in silico methods. The results showed that after optimization of the structures by DMol3 based on DFT-D, the total energies of Nar, GP, CD, and β-CD were calculated at −2100.159, −912.192, −3778.370, and −4273.078 Ha, respectively. The encapsulation energy of Nar on β-CD in the solvent phase was calculated at −93.626 kcal/mol, and the Nar structure was located inside β-CD in solution. The negative interaction energy value for the encapsulation of Nar on β-CD suggests the exothermic adsorption process and a stable structure between Nar and β-CD. Monte Carlo method was applied to obtain adsorption of CS/GP on Nar/β-CD. Its value of the obtained interaction energy was calculated at −1.423 × 103 kcal/mol. The characterization confirmed the formation of a Nar/β-CD inclusion complex. The Zeta potential of the pristine β-CD changed from −4.60 ± 1.1 to −17.60 ± 2.34 mV after interaction with Nar, and the heightened surface negativity can be attributed to the existence of electron-rich naringin molecules, as well as the orientation of the hydroxyl (OH) group of the β-CD toward the surface in an aqueous solution. The porosity of the fabricated hydrogels was in the range of 70−90% and during 14 days around 47.0 ± 3.1% of the pure hydrogel and around 56.4 ± 5.1 of hydrogel nanocomposite was degraded. The MTT assay showed that the hydrogels were biocompatible, and the wound contraction measurement (in an animal model) showed that the closure of the induced wound in the hydrogel nanocomposite treatment was faster than that of the control group (wound without treatment). The results of this study indicate that the developed bioactive wound healing 3D structure, which is composed of a chitosan hydrogel containing a Nar/β-CD inclusion nanocomplex, has potential as an effective material for wound dressing applications.

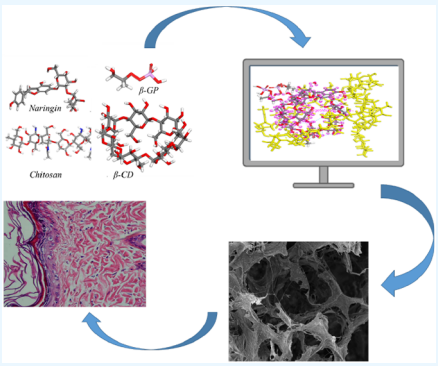

1. INTRODUCTION

The process of skin wound healing is a multifaceted phenomenon that encompasses a series of complex biological mechanisms. Following an injury, a multitude of biological processes are promptly initiated and exhibit a coordinated response. The process of wound repair often results in replacement of the outermost layer of skin, mucous membranes, or fetal skin. The healing of skin involves a nonspecific kind of repair, in which the wound is closed by the formation of scar tissue, a nonfunctional mass of fibrotic tissue.[1,2] It is estimated that almost 400 million individuals experience acute wounds each year, encompassing traumatic wounds, burns, and surgical wounds.[3] Patients with diabetes may experience delayed wound healing, which can lead to a heightened susceptibility to infection and the emergence of potentially severe symptoms. Moreover, chronic wounds exhibit a lack of adherence to a consistent or anticipated trajectory of healing. The management of chronic wounds has, consequently, developed into a distinct field of expertise, whereby medical practitioners frequently employ a range of therapeutic interventions such as engineered skin, growth factors, negative pressure wound therapy, and ECMs.[4−6]

The field of cell and tissue bioengineering has experienced significant advancements, leading to the emergence of a new method for treating wounds.[7,8] Notably, PermaDerm and denovoSkin, two promising innovations, are currently progressing toward clinical application.[9] Nevertheless, the utilization of artificial tissue is restricted due to the experimental character of the treatments and the substantial expenses involved. Inorganic nanoparticle (NP) hybrid materials are commonly employed in the treatment of chronic wounds due to their advantageous characteristics such as low

Received: November 5, 2023
Revised: December 23, 2023
Accepted: January 4, 2024
Published: February 26, 2024

immunogenicity, flexibility, robustness, and scalability.[10] Despite the growing availability of many medicines for the treatment of chronic wounds, the absence of a fully successful treatment remains a significant challenge.[11−13]

In recent years, there has been a growing interest in the application of various natural compounds with possible therapeutic properties in clinical settings.[14−17] In recent years, there has been a growing utilization of natural products in conjunction with various dressings and agents for the management of chronic wounds, leading to favorable outcomes. Naringin (Nar) is a constituent of a traditional Chinese origin that is frequently present in citrus fruits. It is a naturally occurring flavonoid. The compound under consideration possesses a molecular weight of 272.26 P(C15H12O5) and is primarily found in nature in two distinct states: glycosylated, referred to as Nar or naringenin-7-*O*-glucoside, and aglycosylated, known as Nar. Nar has a range of pharmacological characteristics, including anti-inflammatory, antioxidant, antifibrotic, neuroprotective, antibacterial, and anticancer effects.[18−20] Nar has been found to exhibit hepatoprotective effects through the inhibition of oxidative stress and the transforming growth factor (TGF-β) pathway, thereby reducing the transdifferentiation of HSCs and subsequently suppressing liver fibrosis. Nar has been observed to induce cell cycle arrest, specifically in the G and S phases of hepatocellular carcinoma cells. This effect is achieved through the inhibition of cyclin. Additionally, Nar has demonstrated the ability to decrease the metastasis and invasion of pancreatic cells. This is achieved by reducing the expression of vascular endothelial growth factor and downregulating the TGF-β pathway, thereby exhibiting a vascular inhibitory effect.[21,22]

The absorption of Nar by the human gastrointestinal tract is limited with only 15% being absorbed. Furthermore, its bioavailability is notably low, which restricts its practical application. In the field of dermatology, many technologies and methodologies are integrated to optimize the clinical use of Nar due to its limited hydrophobicity.[23−25] An example of a potential therapeutic use for atopic dermatitis is the utilization of a Nar-loaded microsponge gel, which effectively regulates the release of Nar, thus demonstrating its potential as a viable medication option for this condition.[26] The therapeutic efficacy of a sericin gel coated with Nar has been demonstrated to protect against UVB-induced photoaging. Furthermore, it has been observed that the incorporation of Nar into alginate hydrogels has the ability to expedite the process of wound healing in rats. Based on the aforementioned findings, it is postulated that Nar may possess the capacity to potentially serve as a therapeutic agent for the treatment of chronic wounds. Nevertheless, the precise chemical mechanism through which Nar contributes to the process of chronic wound healing remains unclear.[27,28] Nar demonstrates remarkable potential in terms of its anti-inflammatory and wound healing properties. Nevertheless, challenges related to stability and solubility have impeded its widespread adoption in commercial applications.[29,30]

The desirable characteristics of an optimal wound dressing, which contribute to creating an appropriate healing environment, encompass durability, flexibility, water vapor permeability, tissue adhesion, and favorable mechanical qualities. In addition, it is imperative for dressing materials to possess the ability to both hydrate and dehydrate the wound while also ensuring the maintenance of a moist environment. Moreover, these materials should provide protection against infections and prevent the occurrence of maceration.[31−35] Computational simulations have key roles in the development and optimization of the structures and different materials. Different computation methods have been applied to design different structures in different fields.

Hydrogels possess distinctive physical characteristics that render them extensively employed in several biological domains, including tissue engineering, wound management, and drug administration platforms.[36−39] Chitosan (CS) is a copolymer consisting of 2-acetamido-2-deoxy-D-glucopyranose and 2-amino-2-deoxy-D-glucopyranosea, and it is considered a promising candidate for hydrogel formation.[40] The biopolymer possessing a polycationic structure is often derived from alkaline deacetylation of chitin, which ranks as the second most prevalent polysaccharide in the natural world, following cellulose. CS has garnered significant attention in the field of biological applications, including tissue engineering, drug delivery, and wound healing, due to its favorable characteristics such as nontoxicity, biocompatibility, biodegradability, antibacterial properties, and low immunogenicity.[41−43] The objective of this study was to synthesize solid-state inclusion complexes of β-cyclodextrins (β-CDs) with Nar and evaluate their potential application in the development of a hydrogel wound dressing. In this study, molecular modeling and physicochemical characterizations were performed, followed by in vitro and in vivo testing

2. MATERIALS AND METHODS

2.1. Chemicals and Reagents. The β-glycerophosphate disodium salt, Nar, and β-CD used in this study was acquired from Sigma-Aldrich Co. (St. Louis, MO). The medium molecular weight chitosan, with a molecular weight of approximately 210,000 Da and a deacetylation degree of at least 95%, was obtained from Tokyo Chemical Industry Co., Ltd. Acetic acid of analytical grade was provided by Baoxin Bio-Technology Co., Ltd. (Chengdu, China). Unless otherwise specified, all other chemicals were obtained from Invitrogen Life Technologies (Carlsbad, CA).

2.2. Calculation Methods. The electronic structure and energetics of molecules of Nar, β-glycerolphosphate (β-GP), chitosan, and β-CD were obtained by using geometry optimization parameters with the DMol^3 program using density functional theory (DFT) using the Materials Studio 2016 software.[44] These structures were geometrically optimized under DFT-D. DFT-D with the Grimme dispersion correction method was implemented for the van der Waals forces in all calculations. The PBE (Perdew, Burke, and Enzerhof) generalized gradient corrected functional with polarization functions (DNP) were applied for this study.[45,46] In the next stage, MD simulation based on Monte Carlo (MC) was performed by using Universal force field to encapsulation Nar into β-cyclodextrin as well as adsorption of β-GP/chitosan on Nar/β-CD. Electrostatic and van der Waals interactions with a cutoff distance of 12.5 Å were applied for simulation purposes.[47]

2.3. Fabrication of Hydrogels. The procedure for making a 10 mL hydrogel containing CS/CD/Nar involved the execution of the following steps. Initially, a quantity of 200 mg of CS powder was dissolved in 6 mL of acetic acid with a concentration of 0.75% v/v. The mixture was vigorously swirled for a duration of 1 h. Subsequently, a prescribed amount of 20 mg of CD/Nar was dispersed in 2 mL of distilled water and stirred for a period of 4 h. Finally, 600 mg of GP was

https://doi.org/10.1021/acsomega.3c08785
ACS Omega 2024, 9, 10566−10576

dissolved in 2 mL of distilled water. Furthermore, the dispersion of CD/Nar was incorporated into the CS solution and agitated for a duration of 4 h until a thorough amalgamation was achieved. Subsequently, the solution containing the GP solution was incrementally introduced into the mixed solution of CS/CD/Nar while maintaining a consistent stirring rate. The CS/GP hydrogel was made as the control group using the same procedures outlined above, with the exception that the CD/Nar dispersion was substituted with 2 mL of pure water.

2.4. Characterization of Hydrogels. *2.4.1. Gelation Time.* In order to evaluate the gelation time, a volume of 1 mL of a mixture containing CS/CD/Nar cross-linked with β-GP was introduced into a centrifuge tube with a capacity of 15 mL. Subsequently, the tube was subjected to incubation at a temperature of 37 °C. The estimation of gelation resulting from the cross-linking between chains of gelatin was conducted using the vial tilting method.[48]

2.4.2. Swelling Test. In order to assess the fluid retention capacity of the hydrogels, a volume of 1 mL of CS/CD/Nar cross-linked with β-GP was introduced into a centrifuge tube with a capacity of 15 mL. Following complete gelation, the specimen was subjected to freezing at a temperature of −20 °C and subsequently underwent lyophilization. The dried hydrogels were subsequently subjected to incubation in PBS at a temperature of 37 °C. The wet weight of each sample was determined at any time intervals throughout the incubation period. The swelling ratio of hydrogels was determined using the equation provided, where Ws represents the weight of the hydrogel after swelling at different time intervals, and Wd represents the weight of the hydrogel after drying.

2.4.3. Porosity Test. The porosity of the hydrogels was measured using the liquid displacement method.[49] The weight and volume of the lyophilized hydrogel samples were initially measured. Following this, the specimens were fully submerged in a solution of anhydrous ethanol until their mass stabilized at ambient temperature, and the liquid gravimetric $m2$ (g) present on the surface of the material was removed by using a filter paper. The calculation of porosity was performed using the following methodology: The equation for calculating porosity is expressed as follows:

$$\text{Porosity } (\%) = \left(\frac{m2 - m1}{\rho V}\right) \times 100$$

where the variable ρ denotes the density of anhydrous ethanol. The measurements for each substance were conducted in triplicate.

2.4.4. Antioxidant Analysis. The assessment of the antioxidant activity of the synthesized CD/Nar was conducted utilizing the DPPH scavenging assay, which has been previously published.[50,51] In a concise manner, the DPPH solution was evenly dispensed into individual wells of a 96-well plate. Subsequently, varying quantities of the respective samples were introduced into each well. Subsequently, the ultraviolet−visible (UV−vis) absorbance of the samples was determined at a wavelength of 517 nm following an incubation period of 1 h. Finally, a calculation of the percentage of inhibition of free radicals was performed.

2.4.5. Release Kinetics Analysis. To examine the release characteristics, a 15 ml tube was utilized to combine 200 μL of hydrogel and 4 ml of phosphate-buffered saline (pH 7.4). Prior to this, the mixture was subjected to stirring at a temperature of 37 °C and a speed of 100 rpm. The samples were assessed using three separate replicates, each conducted on distinct days. The absorption of Nar was discovered by using ultraviolet spectrophotometry at a wavelength of 425 nm. Finally, the findings were examined, and a graphical representation illustrating the progressive release of Nar was created.

2.5. Cell Viability Test. Fibroblast L929 cells were the experimental model. The lyophilized substance was subjected to cultivation in DMEM supplemented with 10% fetal bovine serum for a duration of 24 h in order to procure an extract with a concentration of 60 mg/mL. L929 cells were inoculated onto 96-well plates with a density of 4000 cells per well and afterward subjected to a 24 h incubation period. Subsequently, the medium was extracted and substituted with 100 μL of a leaching solution. Following a 1-day and 3-day culturing period, the culture medium was substituted with a mixture of 90 μL of medium and 10 μL of MTT reagent. The resulting solution was then incubated within an incubator for a duration of 2 h. Subsequently, the 96-well plate was extracted. The microplate reader (Bio-Rad, United States) was used to measure absorbance values at 590 nm.

2.6. In Vivo Animal Wound Healing Experiments. Female Sprague−Dawley rats, aged 7−8 weeks, were administered anesthesia through the injection of a 3% solution of sodium pentobarbital. Subsequently, the rats were immobilized by being secured onto surgical cork boards. The rats were randomly assigned to two groups: the control group, which received 0.2 mL of normal saline, and the treatment group, which received 0.2 mL of hydrogel. Following the procedure of hair removal, a complete skin lesion with a diameter of 10 mm was induced on the dorsal region of the rat (Figure 1). Subsequently, a volume of 0.2 mL for each material

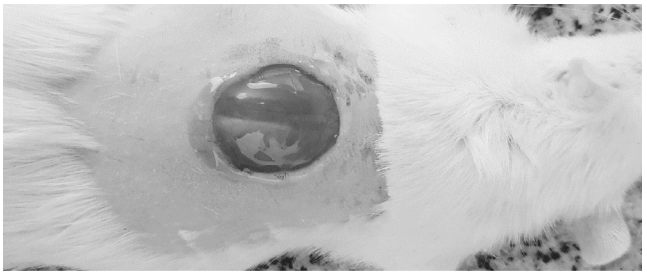

Figure 1. Macroscopic image of the induced wound.

group was administered. Regular provision of water and food was ensured throughout the duration of the study. The percentage reduction in wound area, also known as % wound contraction, was computed for both the control and hydrogel nanocomposite.

$$\%\text{ of wound contraction} = \left(\frac{\text{Wound area on day 0} - \text{wound area on day } n}{\text{wound area on day 0}}\right) \times 100$$

2.6.1. Histopathological Study of Wounds. The wound tissues from each group were collected on the 14th day and subjected to immersion in a 4% paraformaldehyde tissue fixative solution for a duration of 24 h. Subsequently, the tissues were embedded in paraffin and stained using

https://doi.org/10.1021/acsomega.3c08785
ACS Omega 2024, 9, 10566−10576

hematoxylin−eosin (H&E) and Masson's trichrome techniques to generate tissue slices with a thickness of 5 μm. The slices were subjected to imaging and subsequent quantitative analysis using a light microscope. The collagen density and number of new blood vessels in histological skin samples were assessed by using ImageJ software. Regarding animal investigations, a minimum of three biological replicates were carried out in each group, and subsequent staining procedures involving H&E and Masson techniques were completed.

2.7. Statistical Analysis. In all experimental trials, a minimum of three samples were subjected to examination, and the experiments were replicated no less than three times. The findings were reported in terms of means accompanied by their corresponding standard deviations. Statistical significance was denoted by asterisks, with * indicating $p < 0.05$, ** indicating $p < 0.01$, and **** indicating $p < 0.0001$. The data analysis in this study involved the use of either one-way or two-way analysis of variance (ANOVA) in GraphPad Prism 8.0 or Origin software.

3. RESULTS AND DISCUSSION

3.1. DFT and Quantum and Monte Carlo Calculations. *3.1.1. DFT Calculations.* After optimization of the structures by DMol^3 based on DFT-D, the total energies of Nar, *GP*, CD, and β-CD were calculated as −2100.159, −912.192, −3778.370, and −4273.078 Ha, respectively. The computed optimized structures are shown in Figure 2a−d.

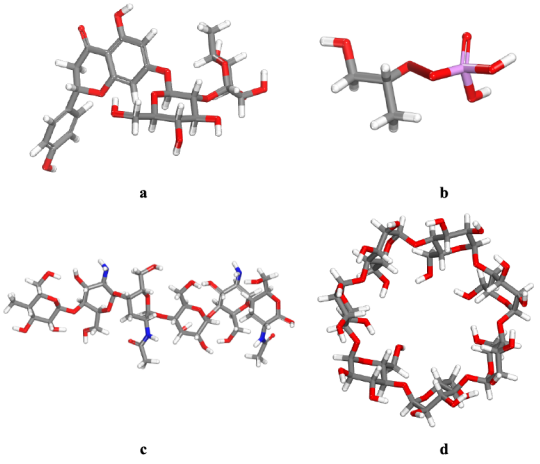

Figure 2. Proposed structures of (a) Nar, (b) β-glycerolphosphate, (c) chitosan, and (d) the side view of β-cyclodextrin.

3.1.2. Encapsulation of Naringin on β-Cyclodextrin. The encapsulation energy of Nar on β-CD in the solvent phase was calculated as −93.626 kcal/mol, and the Nar structure was located inside β-CD in solution. The negative interaction energy value for the encapsulation of Nar on β-CD suggests the exothermic adsorption process and a stable structure between Nar and β-CD (Figure 3a−c). On the contrary, the encapsulation process was more favorable from the energetic viewpoint.[52] In addition, the van der Waals and hydrogen interactions between Nar and β-CD were dominated in the adsorption process.

3.1.3. Adsorption of Naringin β-Cyclodextrin on the Chitosan/β-Glycerophosphate Hydrogel. Recently, MC calculations have been employed to provide molecular level details for the adsorption mechanisms and their orientation.

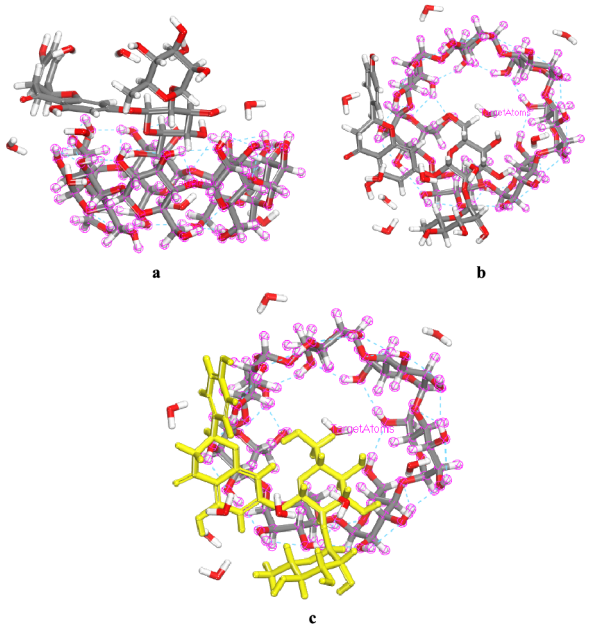

Figure 3. (a−c) The close-up snap shots of equilibrated system based on naringin on β-cyclodextrin resulted by the adsorption locator module in 10 molecules of the solvent.

MC method was applied to obtain adsorption of CS/*GP* on Nar/β-CD. Its value of the obtained interaction energy was calculated as -1.423×10^3 kcal/mol. The adsorption free energy obtained from MC simulation for the Nar/β-CD/CS/*GP* complex was negative, suggesting a spontaneous process, revealing that negative adsorption energy was energetically desirable for adsorption process[53] (Figure 4a−d). Furthermore, the negative value of the Nar/β-CD complex was more stable than that of the CS/*GP* and Nar/β-CD owing to more energy of the Nar/β-CD/CS/*GP* complex as compared with Nar/β-CD complex.[54]

3.2. Properties of Structures. The utilization of β-CD inclusion complexes has proven to be effective in enhancing the solubility, chemical stability, and bioavailability of several chemicals that exhibit poor solubility. Several established techniques have been extensively documented in the literature for the generation of inclusion complexes, including coprecipitation, neutralization, kneading, spray drying, freeze-drying, solvent evaporation, ball-milling, and sealed-heating, as detailed in previous studies.[55] The preparation of the inclusion complex in this investigation was achieved through the utilization of the solvent evaporation technique. During the process of inclusion complex formation, water molecules with a high energy are released from the cavity of the β-CD and Naringin molecules. These water molecules then enter the β-CD cavity, resulting in an apolar−apolar interaction.[56] The synthesized inclusion complex was visualized by using SEM imaging. The results (Figure 7A) showed that the synthesized inclusion complexes have a needle-shaped morphology.

FTIR analysis was conducted to verify the loading of Nar in the β-CD and the formation of the inclusion complex. Figure 5 displays the FTIR spectra of Nar and Nar/β-CD. The FTIR spectra of Nar exhibited distinct peaks at 342 and 2933 cm^{-1}, corresponding to the stretching vibrations of the O−H and C−H bonds, respectively. In addition, the carbonyl (C═) and −C−O− groups exhibited absorption peaks at 1648 and 1041 cm^{-1}, respectively. The FTIR Spectrum of the Nar/β-CD

https://doi.org/10.1021/acsomega.3c08785
ACS Omega 2024, 9, 10566−10576

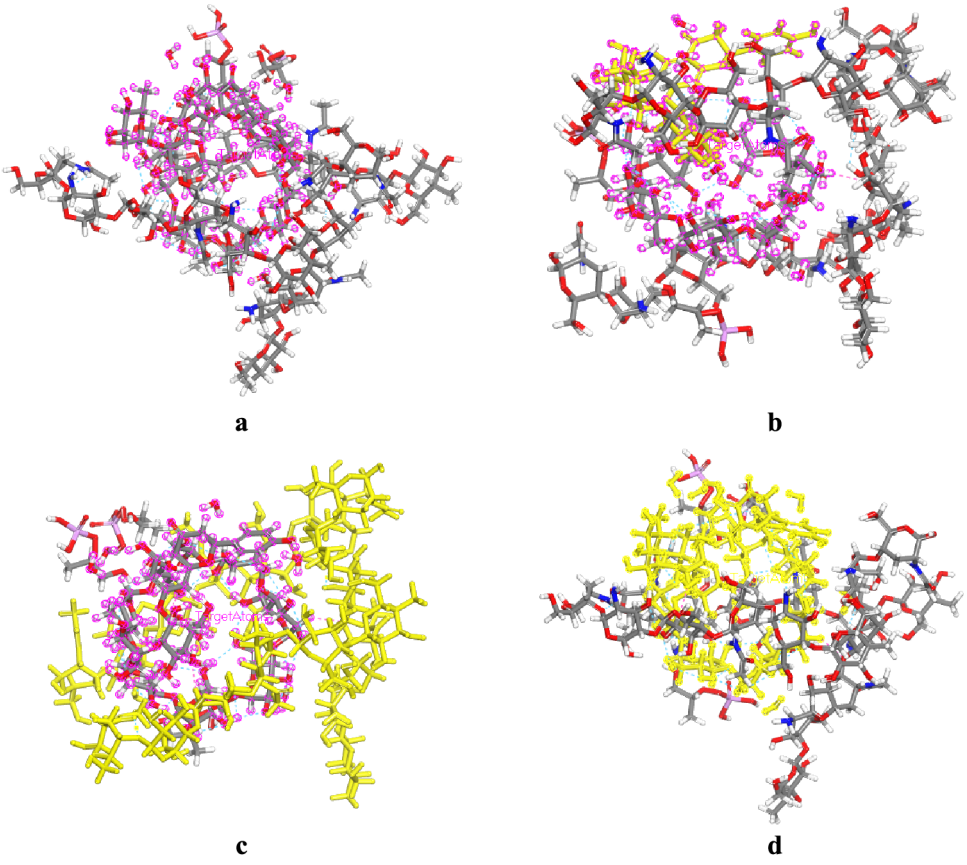

Figure 4. (a-d) Schematic views of equilibrated system based on β-glycerolphosphate/chitosan and Naringin/β-cyclodextrin resulted from the adsorption locator module.

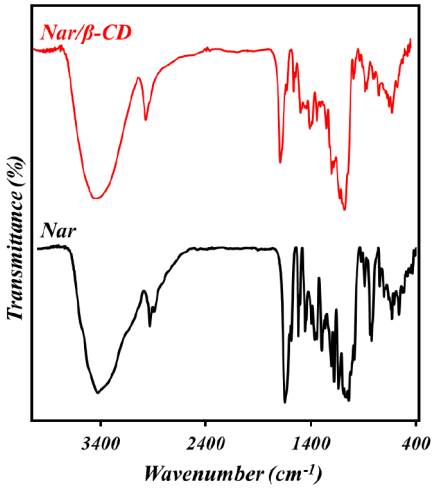

Figure 5. FTIR spectra of pure Nar and Nar/β-CD.

inclusion complex showed a wide peak at 3390 cm^{-1}, showing hydrogen-bonded O−H groups. A peak at 2930 cm^{-1} indicated the vibrational frequency of the C−H bonds. The observed alterations in absorption frequency and intensities of distinctive peaks serve as evidence for the effective loading of Nar with β-CD.

Zeta potential is a crucial factor in nano drug delivery systems that are based on nanoparticles (NPs), and it influences the physical stability of the NPs. The zeta potential of pure β-CD was determined to be −4.60 ± 1.1 mV. However, after loading Nar, the zeta potential increased to −17.60 ± 2.34 mV, as illustrated in Figure 6. A larger zeta potential leads to increased repulsion between particles, resulting in an enhanced resistance to aggregation and prolonged suspension. Furthermore, the zeta potential also influences the therapeutic reactions of medications loaded into

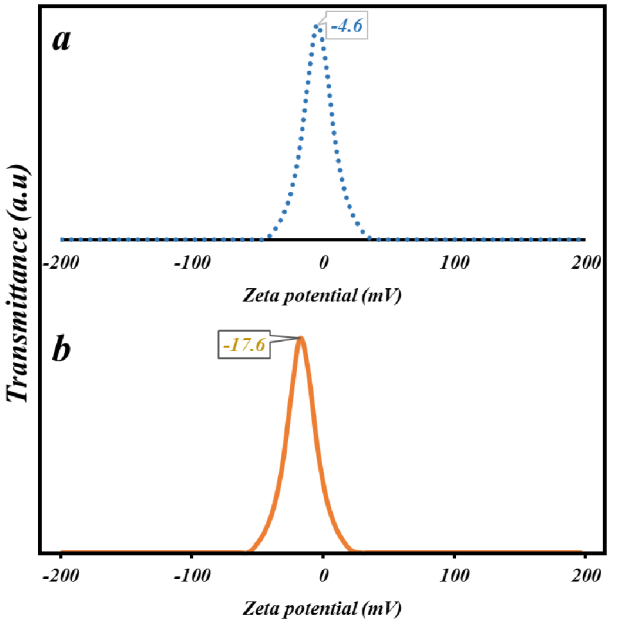

Figure 6. Zeta potentials of (a) pure β-CD and (b) Nar/β-CD.

https://doi.org/10.1021/acsomega.3c08785
ACS Omega 2024, 9, 10566−10576

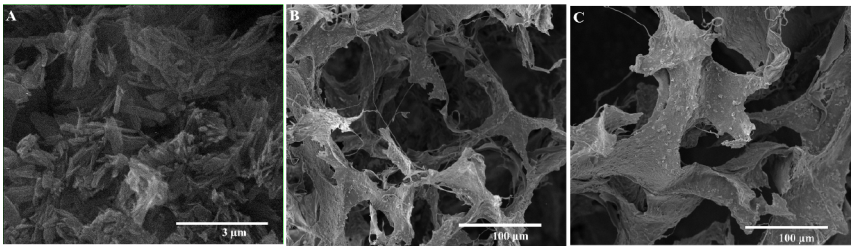

Figure 7. SEM images of (A) the synthesized Nar/β-CD inclusion complex, (B) pure hydrogel, and (C) Nar/β-CD-bearing hydrogels.

nanoparticles as it regulates the electrostatic interactions between the nanoparticles and biological membranes. The enhanced physical stability of the nano formulation and the heightened surface negativity can be attributed to the existence of electron-rich naringin molecules, as well as the orientation of the hydroxyl (OH) group of the β-CD toward the surface in an aqueous solution.

The synthesized inclusion complexes were incorporated into the hydrogel structure and applied as the final wound healing materials. The morphology of the fabricated hydrogels (pure and Nar/β-CD-bearing hydrogels) was observed using SEM imaging. The SEM images (Figure 7A,B) show that the hydrogels have a porous internal structure with interconnected pores.

The fabricated hydrogel was characterized using FTIR spectroscopy, and the results are presented in Figure 8. The results showed that both characteristic peaks of chitosan and the Nar/β-CD inclusion complex are presented in the final formulation (Nar/β-CD-bearing hydrogels).

Moist hydrogel dressings, which belong to the third generation of modern dressings, are derived from a combination of natural polymers (such as agar−agar, gelatin, and pectin) and synthetic polymers (such as poly(vinylpyrrolidone) and poly(ethylene glycol)). These dressings are commercially packaged and undergo sterilization through either electron beam or γ radiation. Hydrogel dressings are commonly employed in the treatment of burn wounds as well as traumatic wounds, ulcerations, and bedsores. Given their notable versatility, they can be employed in various anatomical regions. The removal of the hydrogel dressing is a straightforward and minimally uncomfortable procedure. According to Szewczyk and Cwajda, the process of skin regeneration and repair occurs at a faster rate while utilizing this particular type of dressing as compared to the use of typical dressings.[57] The primary objective of an optimal wound dressing is to maintain a moist environment while simultaneously eliminating excessive effusion and harmful particles.[58] The maintenance of optimal humidity levels facilitated by contemporary wound dressings serves to avoid the formation of a dry scab, which is a characteristic feature of wounds. This, in turn, expedites the healing process of the wounds. The maintenance of a moist wound environment is crucial in alleviating pain by safeguarding and mitigating inflammation at nerve endings inside the nervous system.

The results of the water absorption capacity (Figure 9) showed that the hydrogels absorbed a huge amount of water.

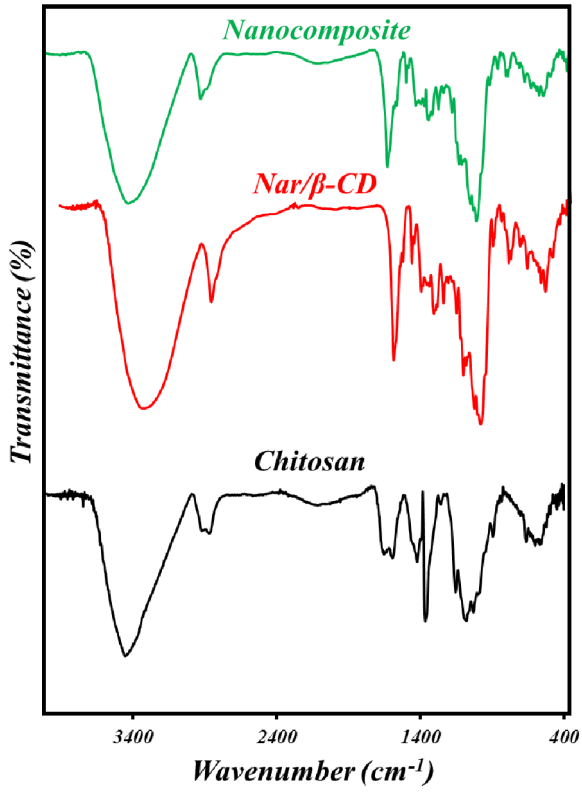

Figure 8. FTIR spectrum of Chitosan, Nar/β-CD inclusion complex, and Nar/β-CD-bearing hydrogels.

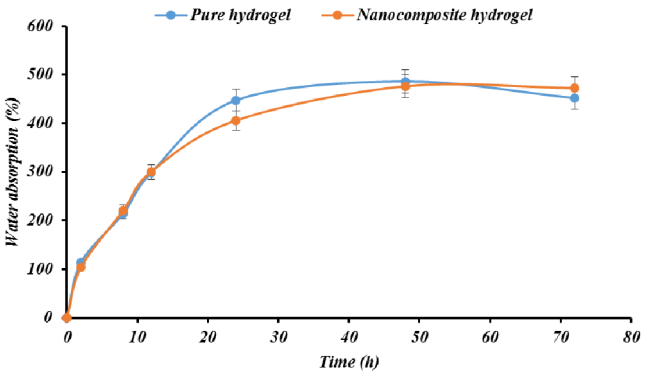

Figure 9. Water absorption and retention capacity of the hydrogels.

Hydrogel wound dressings, composed of a three-dimensional hydrophilic polymer network, have the property of swelling upon contact with water, hence enabling the retention of a significant quantity of water. The hydrogel's gelatinous composition enables it to effectively absorb exudate, sustain optimal wound moisture levels, and facilitate cellular proliferation and migration. Additionally, it possesses effective cleansing qualities by supplying water to necrotic tissues.

The size of pores and the level of porosity play crucial roles in promoting the migration of cells and the formation of blood

https://doi.org/10.1021/acsomega.3c08785
ACS Omega 2024, 9, 10566−10576

vessels. Matrices with a high degree of porosity, ranging from 60% to 90%, offer notable benefits for facilitating the infiltration of cells and the formation of tissues. Additionally, hole diameters within the range of 90−130 μm are deemed adequate for enabling the migration and proliferation of fibroblasts. In addition, previous studies have demonstrated that the presence of hole diameters ranging from 5 to 500 μm plays a crucial role in promoting the effective infiltration of new blood vessels into the interior of the construct. The lack of such vascular invasion has been identified as a contributing factor to cellular demise and tissue necrosis.[59,60] The porosity of the hydrogels was measured using the ethanol displacement method, and the results (Figure 10) showed that the samples

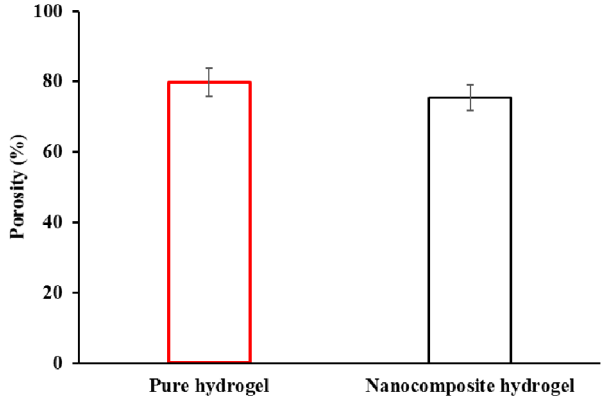

Figure 10. Porosity value of the fabricated hydrogels.

possess a porosity value in the range of 70−90%. The porosity of the pure and nanocomposite hydrogels is strategically situated within this range to facilitate the proliferation of cells and the formation of new blood vessels.

The biodegradation of the fabricated hydrogels was measured in PBS solution (pH: 7.4) during 14 days. The results showed that during 14 days around 47.0 ± 3.1% of the pure hydrogel and around 56.4 ± 5.1 for hydrogel nanocomposite (Figure 11).

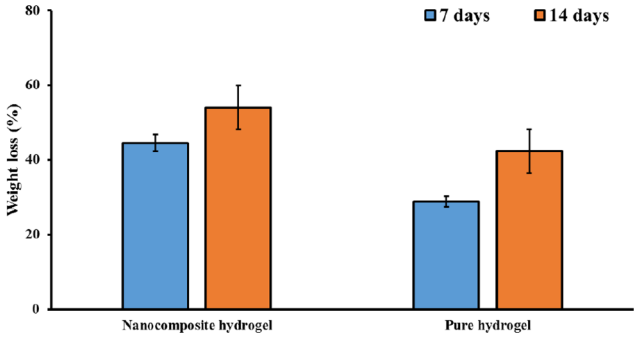

Figure 11. Weight loss value of the fabricated hydrogels.

3.3. Bioactivity Results. Inflammation and infection are primary contributing variables that increase the likelihood of a wound progressing into a chronic state. One potential approach for facilitating the efficient and expeditious healing of wounds is the utilization of degradable wound dressings that incorporate the controlled release of appropriate pharmaceutical agents at the location of the ulcer.[61] Despite the successful utilization of hydrogels in many preclinical wound models, these materials do possess a notable limitation when employed as delivery vehicles. The significant release of the drug is attributed to the characteristics of its production and composition, which include partial nonloading of the drug or its quick efflux from the gel when it undergoes swelling.[48] This phenomenon might pose significant risks, as it may result in heightened systemic drug concentrations, hence increasing the likelihood of adverse consequences occurring at remote sites. Our results (Figure 12) showed that around 80% of the loaded drug was released during the first 10 h of the study.

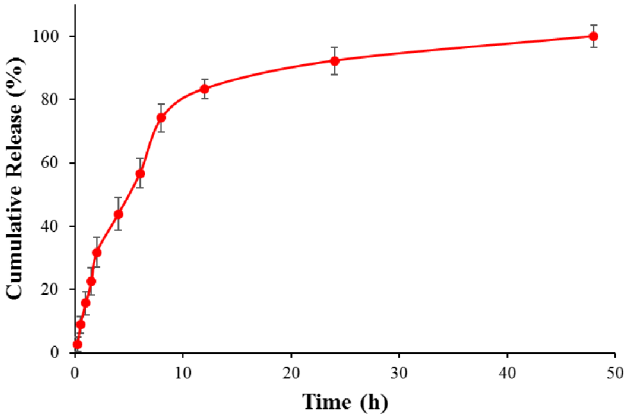

Figure 12. Release profile of Naringin from the nanocomposite hydrogel.

The intricate regulation of wound healing processes is contingent upon maintaining a precise equilibrium between oxidative stress and antioxidants. The physiological process of wound healing typically relies on minimal levels of reactive oxygen species and oxidative stress. However, excessive exposure to oxidative stress can result in a compromised wound healing. It is hypothesized that antioxidants play a role in regulating oxidative stress associated with wounds, potentially leading to an expedited wound healing process.[62] The antioxidant capacity of the synthesized Nar/β-CD inclusion complex was evaluated using the DPPH assay technique, and the results are presented in Figure 13. Regarding the matter at hand, it was observed that an elevation in the concentration of Naringin led to a corresponding rise in the percentage inhibition due to an augmented radical scavenging activity. This activity, in turn, reduces the presence of Naringin in the test solution. The results obtained were consistent with the findings of prior

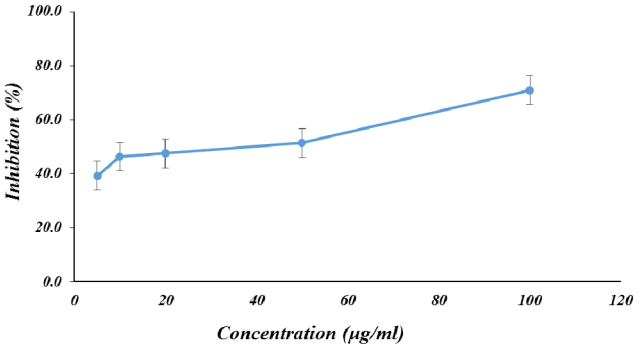

Figure 13. Antioxidant activity of the Nar/β-CD inclusion complex. Measured by a DPPH assay kit.

https://doi.org/10.1021/acsomega.3c08785
ACS Omega 2024, 9, 10566−10576

studies.[63] The results obtained in this study provide confirmation that the developed methodology may be effectively employed for the estimation of the antioxidant activity of naringin.

One of the most important requirements of wound dressings is biocompatibility. Viability of cells on the scaffolds can reveal the biocompatibility of the fabricated dressings.[64] The viability of the cells on the fabricated hydrogels (pure and nanocomposite hydrogels) was evaluated using the MTT assay, and the results are presented in Figure 14. The results showed that

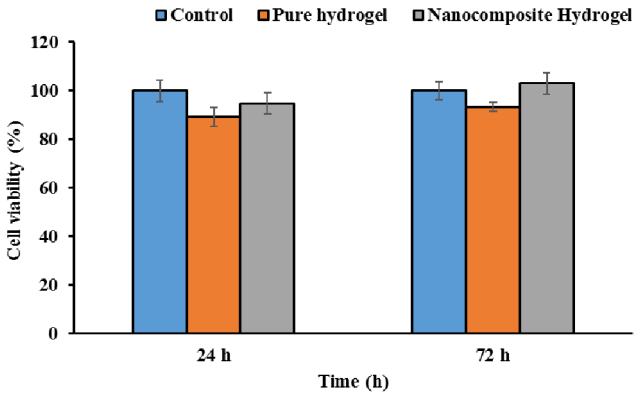

Figure 14. Viability of cells on the hydrogels, measured by the MTT assay.

the fabricated hydrogel did not induce any adverse effect of the viability of cells. Moreover, it can be seen that the incorporation of Nar/β-CD inclusion complex improved the viability of the cells.

3.4. Animal Study Results. The wound healing potential of the fabricated hydrogels was investigated in a full-thickness animal model. The treatment using the hydrogel nanocomposite lasted 14 days. The healing outcomes were evaluated using the wound contraction profile during treatment (Figure 15) and the histological evaluations (H&E and

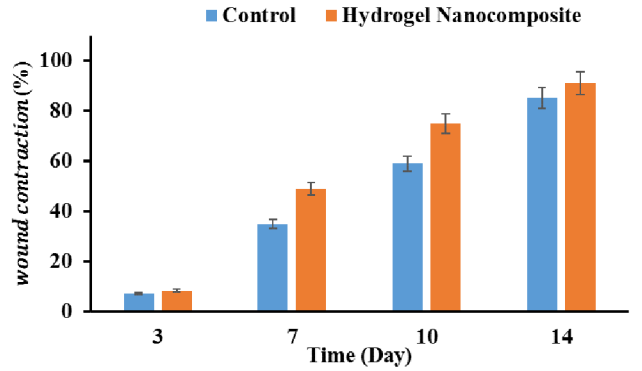

Figure 15. Wound contract during the treatment. Control: wound without treatment.

MT staining). The wound contraction measurement showed that the closure of the induced wound in the hydrogel nanocomposite treatment was faster than that of the control group (wound without treatment).

The results (Figure 16) showed that the treatment significantly improved the healing process of the wound compared with the control group (wound treated with standard gauze dressing). In the control group (Figure

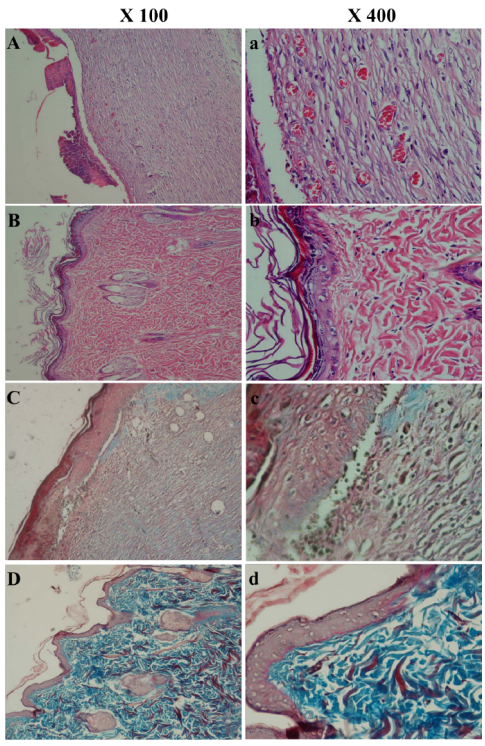

Figure 16. Histopathological characteristics of the wounds. (A,a) H&E staining of the control group, (B,b) H&E staining of the hydrogel-treated group, (C,c) MT staining of the control group, and (D,d) MT staining of the hydrogel-treated group.

16Aa,Cc), the epyderal layer was not formed correctly, and the wound surface is covered scabs. While, the treatment using the hydrogel induced the formation of an effective epidermal layer (Figure 16Bb,Dd). Moreover, hydrogel induced formation of hair follicles and sebaceous gland, while these normal skin features are not apparent in the control group.

4. CONCLUSION

The development of a potentially effective technique for skin regeneration is a significant challenge within the field of biomedical research. The user's text is too short to be rewritten in an academic manner. The process of wound healing is significantly impacted by the reciprocal interaction between many crucial cell types and their cellular components. Wound healing is a multifaceted process that encompasses various interconnected mechanisms including hemostasis, inflammation, proliferation, and remodeling. The duration of each phase of wound healing is contingent on the extent and location of the wound. Wound dressing materials, also known as bioactive materials, play a crucial role in facilitating the healing process. They achieve this by effectively managing moisture levels, facilitating gas exchange, regulating the excessive release of exudates, and mitigating the risk of wound infection, all of which significantly impact the overall healing trajectory.

Nar is a prominent flavanone glycoside that has been extensively studied for its pharmacological properties. These properties include antimicrobial, antimutagenic, anti-inflammatory, cholesterol-lowering, antioxidant, antiulcer, anticancer, antiatherogenic, hepatoprotective, cardioprotective, renoprotective, and neuroprotective effects. Unfortunately, the clinical significance of Nar is constrained by its limited solubility and inadequate bioavailability due to its predominantly hydro-

https://doi.org/10.1021/acsomega.3c08785
ACS Omega 2024, 9, 10566−10576

phobic ring shape. This study investigates the potential of β-CD as excipients for improving the solubility and oral absorption of flavonoid compound. CDs encompass a group of cyclic oligosaccharides that possess a distinctive three-dimensional toroid configuration, hence establishing a cavity capable of accommodating diminutive hydrophobic molecules, such as cholesterol or steroids. CDs can thus serve as excipients to enhance the solubility of hydrophobic medicines exhibiting comparable structural characteristics. In a previous study, it was observed that the bioavailability of rutin, a flavonoid-glycoside having a structural resemblance to naringin, was notably increased through the process of complexation with 2-hydroxypropyl-β-CD. In this study, we present evidence supporting the enhancement of the bioactivities of Nar through the utilization of β-CD.

The synthesized Nar/β-CD inclusion complexes were incorporated into the chitosan hydrogel and applied as the wound dressing material. The results showed that the fabricated hydrogels exhibited outstanding physical and biological properties beneficial for wound healing and regenerative medicine applications.

■ ASSOCIATED CONTENT

Data Availability Statement

The data sets used and/or analyzed during the current study are available from the corresponding author on reasonable request.

■ AUTHOR INFORMATION

Corresponding Author

Jianhai Bi − *Department of Plastic and Aesthetic Surgery, Shandong Provincial Hospital Affiliated to Shandong First Medical University, Jinan 250021 Shandong, China; Medical Science and Technology Innovation Center, Shandong First Medical University & Shandong Academy of Medical Sciences, Jinan 250021 Shandong, China;* orcid.org/0000-0001-6482-5819; Email: bijianhai@126.com

Authors

Donghui Bian − *Department of Burns and Plastic Surgery, 960 Hospital of the People's Liberation Army, Jinan 250031, China*

Younes Pilehvar − *Cellular and Molecular Research Center, Cellular and Molecular Medicine Research Institute, Urmia University of Medical Sciences, Urmia 571478334, Iran*

Sanaz Kousha − *Department of Food Hygiene, Science and Research Branch, Islamic Azad University, Tehran 1477893855, Iran*

Complete contact information is available at: https://pubs.acs.org/10.1021/acsomega.3c08785

Author Contributions

Donghui Bian was responsible for the methodology, formal analysis, and writing−review and editing. Sanaz Kousha was responsible for the formal analysis, investigation, and writing−review and editing. Younes Pilehvar was responsible for the writing−original draft and writing−review and editing. Jianhai Bi was responsible for the conceptualization, data curation, writing−review and editing, supervision, project administration, and funding acquisition.

Notes

The authors declare no competing financial interest.

■ ACKNOWLEDGMENTS

We would like to express sincere appreciation toward Shandong Province Traditional Chinese Medicine Health Science and Technology Plan Development Project (202204031073) and Special funds for Shandong Province Wound Repair and Rehabilitation Engineering Technology Research Center, Mount Taishan Scholar Distinguished Expert Fund (No. ts201511100). All animal experimental procedures were conducted according to the ethical regulations of the Department of Plastic and Aesthetic Surgery, Shandong Provincial Hospital Affiliated to Shandong First Medical University, China.

■ REFERENCES

(1) Arezoumand, K. S.; Alizadeh, E.; Esmaeillou, M.; Ghasemi, M.; Alipour, S.; Pilehvar-Soltanahmadi, Y.; Zarghami, N. The emu oil emulsified in egg lecithin and butylated hydroxytoluene enhanced the proliferation, stemness gene expression, and in vitro wound healing of adipose-derived stem cells. *In Vitro Cell. Dev. Biol.: Animal* **2018**, *54*, 205−216.

(2) Pilehvar-Soltanahmadi, Y.; Akbarzadeh, A.; Moazzez-Lalaklo, N.; Zarghami, N. An update on clinical applications of electrospun nanofibers for skin bioengineering. *Artif. Cells Nanomed. Biotechnol.* **2016**, *44*, 1350−1364.

(3) Sen, C. K. Human wounds and its burden: an updated compendium of estimates. *Advances in Wound Care* **2019**, *8*, 39−48.

(4) Greenhalgh, D. G. Wound healing and diabetes mellitus. *Clinics in Plastic Surgery* **2003**, *30*, 37−45.

(5) Okonkwo, U. A.; DiPietro, L. A. Diabetes and wound angiogenesis. *Int. J. Mol. Sci.* **2017**, *18*, 1419.

(6) Falanga, V. Wound healing and its impairment in the diabetic foot. *Lancet* **2005**, *366*, 1736−1743.

(7) Pourpirali, R.; Mahmoudnezhad, A.; Oroojalian, F.; Zarghami, N.; Pilehvar, Y. Prolonged proliferation and delayed senescence of the adipose-derived stem cells grown on the electrospun composite nanofiber co-encapsulated with TiO2 nanoparticles and metformin-loaded mesoporous silica nanoparticles. *Int. J. Pharm.* **2021**, *604*, 120733.

(8) Sadeghi-Soureh, S.; Jafari, R.; Gholikhani-Darbroud, R.; Pilehvar-Soltanahmadi, Y. Potential of Chrysin-loaded PCL/gelatin nanofibers for modulation of macrophage functional polarity towards anti-inflammatory/pro-regenerative phenotype. *J. Drug Delivery Sci. Technol.* **2020**, *58*, 101802.

(9) Varkey, M.; Ding, J.; Tredget, E. E. Advances in Skin Substitutes—Potential of Tissue Engineered Skin for Facilitating Anti-Fibrotic Healing. *J. Funct. Biomater.* **2015**, *6*, 547−563.

(10) Serati-Nouri, H.; Mahmoudnezhad, A.; Bayrami, M.; Sanajou, D.; Tozihi, M.; Roshangar, L.; Pilehvar, Y.; Zarghami, N. Sustained delivery efficiency of curcumin through ZSM-5 nanozeolites/electrospun nanofibers for counteracting senescence of human adipose-derived stem cells. *J. Drug Delivery Sci. Technol.* **2021**, *66*, 102902.

(11) Stamatialis, D. F.; Papenburg, B. J.; Gironés, M.; Saiful, S.; Bettahalli, S. N. M.; Schmitmeier, S.; Wessling, M. Medical applications of membranes: Drug delivery, artificial organs and tissue engineering. *J. Membr. Sci.* **2008**, *308*, 1−34.

(12) Nethi, S. K.; Das, S.; Patra, C. R.; Mukherjee, S. Recent advances in inorganic nanomaterials for wound-healing applications. *Biomater. Sci.* **2019**, *7*, 2652−2674.

(13) Matter, M. T.; Probst, S.; Läuchli, S.; Herrmann, I. Uniting drug and delivery: metal oxide hybrid nanotherapeutics for skin wound care. *Pharmaceutics* **2020**, *12*, 780.

(14) Zamani, R.; Pilehvar-Soltanahmadi, Y.; Alizadeh, E.; Zarghami, N. Macrophage repolarization using emu oil-based electrospun nanofibers: possible application in regenerative medicine. *Artif. Cells Nanomed. Biotechnol.* **2018**, *46*, 1258−1265.

(15) Dadashpour, M.; Pilehvar-Soltanahmadi, Y.; Zarghami, N.; Firouzi-Amandi, A.; Pourhassan-Moghaddam, M.; Nouri, M. Emerg-

ing importance of phytochemicals in regulation of stem cells fate via signaling pathways. *Phytotherapy Res.* **2017**, *31*, 1651−1668.
(16) Sun, S.-J.; Deng, P.; Peng, C.-E.; Ji, H.-Y.; Mao, L.-F.; Peng, L.-Z. Extraction, structure and immunoregulatory activity of low molecular weight polysaccharide from Dendrobium officinale. *Polymers* **2022**, *14*, 2899.
(17) Liu, Y.; Li, H.; Wang, X.; Huang, J.; Zhao, D.; Tan, Y.; Zhang, Z.; Zhang, Z.; Zhu, L.; Wu, B.; Chen, Z.; Peng, W. Anti-Alzheimers molecular mechanism of icariin: insights from gut microbiota, metabolomics, and network pharmacology. *J. Transl. Med.* **2023**, *21*, 277.
(18) Qu, H.; Zhang, Y.; Qu, B.; Cheng, J.; Liu, S.; Feng, S.; Wang, Q.; Zhao, Y. Novel immunoassay and rapid immunoaffinity chromatography method for the detection and selective extraction of naringin in Citrus aurantium. *J. Sep. Sci.* **2016**, *39*, 1389−1398.
(19) Xu, C.; Huang, X.; Huang, Y.; Liu, X.; Wu, M.; Wang, J.; Duan, X. Naringin induces apoptosis of gastric carcinoma cells via blocking the PI3K/AKT pathway and activating pro-death autophagy. *Mol. Med. Rep.* **2021**, *24*, 1−10.
(20) Da Pozzo, E. The citrus flavanone naringenin protects myocardial cells against age-associated damage. *Oxid. Med. Cell. Longevity* **2017**, *2017*, 1210675.
(21) Wu, Y. Naringin ameliorates monocrotaline-induced pulmonary arterial hypertension through endothelial-to-mesenchymal transition inhibition. *Front. Pharmacol.* **2021**, *12*, 696135.
(22) Du, Y.; Ma, J.; Fan, Y.; Wang, X.; Zheng, S.; Feng, J.; Li, J.; Fan, Z.; Li, G.; Ye, Q. Naringenin: A promising therapeutic agent against organ fibrosis. *Oxid. Med. Cell. Longevity* **2021**, *2021*, 1−13.
(23) Orrego-Lagaron, N.; Martínez-Huélamo, M.; Quifer-Rada, P.; Lamuela-Raventos, R. M.; Escribano-Ferrer, E. Absorption and disposition of naringenin and quercetin after simultaneous administration via intestinal perfusion in mice. *Food Funct.* **2016**, *7*, 3880−3889.
(24) Krogholm, K. S.; Bredsdorff, L.; Knuthsen, P.; Haraldsdóttir, J.; Rasmussen, S. E. Relative bioavailability of the flavonoids quercetin, hesperetin and naringenin given simultaneously through diet. *Eur. J. Clin. Nutr.* **2010**, *64*, 432−435.
(25) Chen, M.; Li, R.; Gao, Y.; Zheng, Y.; Liao, L.; Cao, Y.; Li, J.; Zhou, W. Encapsulation of hydrophobic and low-soluble polyphenols into nanoliposomes by pH-driven method: Naringenin and naringin as model compounds. *Foods* **2021**, *10*, 963.
(26) Sun, R.; Liu, C.; Liu, J.; Yin, S.; Song, R.; Ma, J.; Cao, G.; Lu, Y.; Zhang, G.; Wu, Z. Integrated network pharmacology and experimental validation to explore the mechanisms underlying naringenin treatment of chronic wounds. *Sci. Rep.* **2023**, *13*, 132.
(27) Parashar, P.; Pal, S.; Dwivedi, M.; Saraf, S. A. Augmented therapeutic efficacy of naringenin through microemulsion-loaded sericin gel against uvb-induced photoaging. *AAPS PharmSciTech* **2020**, *21*, 1−13.
(28) Sharma, S.; Hafeez, A.; Usmani, S. A. Nanoformulation approaches of naringenin-an updated review on leveraging pharmaceutical and preclinical attributes from the bioactive. *J. Drug Delivery Sci. Technol.* **2022**, *76*, 103724.
(29) Hussain, K.; Ali, I.; Ullah, S.; Imran, M.; Parveen, S.; Kanwal, T.; Shah, S. A.; Saifullah, S.; Shah, M. R. Enhanced antibacterial potential of naringin loaded β cyclodextrin nanoparticles. *J. Clust. Sci.* **2022**, *33*, 339−348.
(30) Mo, Y.; Zhao, F.; Lin, Z.; Cao, X.; Chen, D.; Chen, X. Local delivery of naringin in beta-cyclodextrin modified mesoporous bioactive glass promotes bone regeneration: from anti-inflammatory to synergistic osteogenesis and osteoclastogenesis. *Biomater. Sci.* **2022**, *10*, 1697−1712.
(31) Abazari, M.; Akbari, T.; Hasani, M.; Sharifikolouei, E.; Raoufi, M.; Foroumadi, A.; Sharifzadeh, M.; Firoozpour, L.; Khoobi, M. Polysaccharide-based hydrogels containing herbal extracts for wound healing applications. *Carbohydr. Polym.* **2022**, *294*, 119808.
(32) Deng, L.; Wang, B.; Li, W.; Han, Z.; Chen, S.; Wang, H. Bacterial cellulose reinforced chitosan-based hydrogel with highly efficient self-healing and enhanced antibacterial activity for wound healing. *Int. J. Biol. Macromol.* **2022**, *217*, 77−87.
(33) Wang, Y.; Zhai, W.; Li, J.; Liu, H.; Li, C.; Li, J. Friction behavior of biodegradable electrospun polyester nanofibrous membranes. *Tribol. Int.* **2023**, *188*, 108891.
(34) Yuan, J.; Wang, Y.; Yang, W.; Li, X.; Tao, K.; He, W.; Yan, J. Biomimetic peptide dynamic hydrogel inspired by humanized defensin nanonets as the wound-healing gel coating. *Chem. Eng. J.* **2023**, *470*, 144266.
(35) Huang, Y.; Mu, L.; Zhao, X.; Han, Y.; Guo, B. Bacterial growth-induced tobramycin smart release self-healing hydrogel for Pseudomonas aeruginosa-infected burn wound healing. *ACS Nano* **2022**, *16*, 13022−13036.
(36) Ho, T.-C.; Chang, C.-C.; Chan, H.-P.; Chung, T.-W.; Shu, C.-W.; Chuang, K.-P.; Duh, T.-H.; Yang, M.-H.; Tyan, Y.-C. Hydrogels: Properties and applications in biomedicine. *Molecules* **2022**, *27*, 2902.
(37) Hong, Y.; Lin, Z.; Yang, Y.; Jiang, T.; Shang, J.; Luo, Z. Biocompatible conductive hydrogels: applications in the field of biomedicine. *Int. J. Mol. Sci.* **2022**, *23*, 4578.
(38) Liu, J.; Zhou, Y.; Lu, J.; Cai, R.; Zhao, T.; Chen, Y.; Zhang, M.; Lu, X.; Chen, Y. Injectable, tough and adhesive zwitterionic hydrogels for 3D-printed wearable strain sensors. *Chem. Eng. J.* **2023**, *475*, 146340.
(39) Yu, R.; Yang, Y.; He, J.; Li, M.; Guo, B. Novel supramolecular self-healing silk fibroin-based hydrogel via host−guest interaction as wound dressing to enhance wound healing. *Chem. Eng. J.* **2021**, *417*, 128278.
(40) Mehrabi, M.; Dounighi, N. M.; Rezayat Sorkhabadi, S. M.; Doroud, D.; Amani, A.; Khoobi, M.; Ajdary, S.; Pilehvar-Soltanahmadi, Y. Development and physicochemical, toxicity and immunogenicity assessments of recombinant hepatitis B surface antigen (rHBsAg) entrapped in chitosan and mannosylated chitosan nanoparticles: as a novel vaccine delivery system and adjuvant. *Artif. Cells, Nanomed., Biotechnol.* **2018**, *46*, 230−240.
(41) Riva, R.; Ragelle, H.; des Rieux, A.; Duhem, N.; Jerome, C.; Préat, V. Chitosan and chitosan derivatives in drug delivery and tissue engineering; In *Chitosan for Biomaterials II*; Springer, 2011; pp 19−44
(42) Zhao, X.; Li, P.; Guo, B.; Ma, P. X. Antibacterial and conductive injectable hydrogels based on quaternized chitosan-graft-polyaniline/oxidized dextran for tissue engineering. *Acta Biomater.* **2015**, *26*, 236−248.
(43) Rahmanian-Devin, P.; Baradaran Rahimi, V.; Askari, V. R. Thermosensitive chitosan-β-glycerophosphate hydrogels as targeted drug delivery systems: An overview on preparation and their applications. *Adv. Pharmacol. Pharm. Sci.* **2021**, *2021*, 6640893.
(44) Ighnih, H.; Haounati, R.; Eshaghi Malekshah, R.; Ouachtak, H.; Toubi, Y.; Alakhras, F.; Jada, A.; Ait Addi, A. Sunlight driven photocatalytic degradation of RhB dye using composite of bismuth oxy-bromide kaolinite BiOBr@ Kaol: Experimental and molecular dynamic simulation studies. *J. Photochem. Photobiol., A* **2023**, *445*, 115071.
(45) Dorairaj, D. P.; Haribabu, J.; Dharmasivam, M.; Malekshah, R. E.; Mohamed Subarkhan, M. K.; Echeverria, C.; Karvembu, R. Ru (II)-p-Cymene Complexes of Furoylthiourea Ligands for Anticancer Applications against Breast Cancer Cells. *Inorg. Chem.* **2023**, *62*, 11761−11774.
(46) He, Z.; Yue, C.; Chen, X.; Li, X.; Zhang, L.; Tan, S.; Yi, X.; Luo, G.; Zhou, Y. Integrative Analysis Identified CD38 As a Key Node That Correlates Highly with Immunophenotype, Chemoradiotherapy Resistance, And Prognosis of Head and Neck Cancer. *J. Cancer* **2023**, *14*, 72.
(47) Feng, L.; Liu, J.; Abu-Hamdeh, N. H.; Bezzina, S.; Eshaghi Malekshah, R. Molecular dynamics and quantum simulation of different cationic dyes removal from contaminated water using UiO-66 (Zr)-(COOH)2 metal−organic framework. *J. Mol. Liq.* **2022**, *349*, 118085.
(48) Tsai, C.-C.; Hong, Y.-J.; Lee, R. J.; Cheng, N.-C.; Yu, J. Enhancement of human adipose-derived stem cell spheroid differ-

https://doi.org/10.1021/acsomega.3c08785
ACS Omega 2024, 9, 10566−10576

entiation in an in situ enzyme-crosslinked gelatin hydrogel. *J. Mater. Chem. B* **2019**, *7*, 1064−1075.
(49) Ponrasu, T.; Veerasubramanian, P. K.; Kannan, R.; Gopika, S.; Suguna, L.; Muthuvijayan, V. Morin incorporated polysaccharide−protein (psyllium−keratin) hydrogel scaffolds accelerate diabetic wound healing in Wistar rats. *RSC Adv.* **2018**, *8*, 2305−2314.
(50) Khorrami, S.; Zarrabi, A.; Khaleghi, M.; Danaei, M.; Mozafari, M. R. Selective cytotoxicity of green synthesized silver nanoparticles against the MCF-7 tumor cell line and their enhanced antioxidant and antimicrobial properties. *Int. J. Nanomed.* **2018**, *13*, 8013−8024.
(51) Khorrami, S.; Zarepour, A.; Zarrabi, A. Green synthesis of silver nanoparticles at low temperature in a fast pace with unique DPPH radical scavenging and selective cytotoxicity against MCF-7 and BT-20 tumor cell lines. *Biotechnol. Rep.* **2019**, *24*, No. e00393.
(52) Haounati, R.; Ighnih, H.; Malekshah, R. E.; Alahiane, S.; Alakhras, F.; Alabbad, E.; Alghamdi, H.; Ouachtak, H.; Addi, A. A.; Jada, A. Exploring ZnO/Montmorillonite Photocatalysts for the Removal of Hazardous RhB Dye: A Combined Study using Molecular Dynamics Simulations and Experiments. *Mater. Today Commun.* **2023**, *35*, 105915.
(53) Haounati, R.; Ighnih, H.; Ouachtak, H.; Malekshah, R. E.; Hafid, N.; Jada, A.; Ait Addi, A. Z-Scheme g-C3N4/Fe3O4/Ag3PO4 @Sep magnetic nanocomposites as heterojunction photocatalysts for green malachite degradation and dynamic molecular studies. *Colloids Surf., A* **2023**, *671*, 131509.
(54) Ganjali Koli, M.; Eshaghi Malekshah, R.; Hajiabadi, H. Insights from molecular dynamics and DFT calculations into the interaction of 1, 4-benzodiazepines with 2-hydroxypropyl-βCD in a theoretical study. *Sci. Rep.* **2023**, *13*, 9866.
(55) Louiz, S.; Labiadh, H.; Abderrahim, R. Synthesis and spectroscopy studies of the inclusion complex of 3-amino-5-methyl pyrazole with beta-cyclodextrin. *Spectrochim. Acta, Part A* **2015**, *134*, 276−282.
(56) Rachmawati, H.; Edityaningrum, C. A.; Mauludin, R. Molecular Inclusion Complex of Curcumin−β-Cyclodextrin Nanoparticle to Enhance Curcumin Skin Permeability from Hydrophilic Matrix Gel. *AAPS PharmSciTech* **2013**, *14*, 1303−1312.
(57) Bartkowiakb, G.; Frydrych, I. 23 - Superabsorbents and their medical applications. Bartels, V. T., Ed.; In *Handbook of Medical Textiles*; Woodhead Publishing, 2011; pp 505−546. DOI: 10.1533/9780857093691.4.505
(58) Pilehvar-Soltanahmadi, Y. An overview on application of natural substances incorporated with electrospun nanofibrous scaffolds to development of innovative wound dressings. *Mini-Rev. Med. Chem.* **2018**, *18*, 414−427.
(59) MacEwan, M. R.; MacEwan, S.; Kovacs, T. R.; Batts, J. What makes the optimal wound healing material? A review of current science and introduction of a synthetic nanofabricated wound care scaffold. *Cureus* **2017**, *9*, No. e1736.
(60) Mousavi, S. M.; Zarei, M.; Hashemi, S. A.; Ramakrishna, S.; Chiang, W.-H.; Lai, C. W.; Gholami, A.; Omidifar, N.; Shokripour, M. Asymmetric membranes: A potential scaffold for wound healing applications. *Symmetry* **2020**, *12*, 1100.
(61) Heydari, P. Comparing the wound healing effect of a controlled release wound dressing containing curcumin/ciprofloxacin and simvastatin/ciprofloxacin in a rat model: A preclinical study. *J. Biomed. Mater. Res., Part A* **2022**, *110*, 341−352.
(62) Fitzmaurice, S.; Sivamani, R.; Isseroff, R. Antioxidant therapies for wound healing: a clinical guide to currently commercially available products. *Skin Pharmacol. Physiol.* **2011**, *24*, 113−126.
(63) Kumari, S. D.; Chevala, N. T.; Jitta, S. R.; Kumar, L.; Verma, R.; Jose, J. Design and development of naringin-loaded proposomal gel for wound healing. *Journal of Cosmetic Dermatology* **2022**, *21*, 5187−5202.
(64) Wang, Y.; Zhai, W.; Cheng, S.; Li, J.; Zhang, H. Surface-functionalized design of blood-contacting biomaterials for preventing coagulation and promoting hemostasis. *Friction* **2023**, *11*, 1371−1394.

https://doi.org/10.1021/acsomega.3c08785
ACS Omega 2024, 9, 10566−10576